IJMMM International Journal of Minerals, Metallurgy and Materials 矿物冶金与材料学报（英文版）

Bullet-like vanadium-based MOFs as a highly active catalyst for promoting the hydrogen storage property in MgH_2

Zhiyu Lu, Jiahuan He, Mengchen Song, Yan Zhang, Fuying Wu, Jiaguang Zheng, Liuting Zhang, and Lixin Chen

Cite this article as:
Zhiyu Lu, Jiahuan He, Mengchen Song, Yan Zhang, Fuying Wu, Jiaguang Zheng, Liuting Zhang, and Lixin Chen, Bullet-like vanadium-based MOFs as a highly active catalyst for promoting the hydrogen storage property in MgH_2, *Int. J. Miner. Metall. Mater.*, 30(2023), No. 1, pp. 44-53. https://doi.org/10.1007/s12613-021-2372-5

View the article online at SpringerLink or IJMMM Webpage.

International Journal of Minerals, Metallurgy and Materials
Volume 30, Number 1, January 2023, Page 44
https://doi.org/10.1007/s12613-021-2372-5

Bullet-like vanadium-based MOFs as a highly active catalyst for promoting the hydrogen storage property in MgH_2

Zhiyu Lu[1),*], *Jiahuan He*[3),*], *Mengchen Song*[1)], *Yan Zhang*[1)], *Fuying Wu*[2)], *Jiaguang Zheng*[1)], *Liuting Zhang*[1),✉], *and Lixin Chen*[3)]

1) School of Energy and Power, Jiangsu University of Science and Technology, Zhenjiang 212003, China
2) Instrumental Analysis Center, Jiangsu University of Science and Technology, Zhenjiang 212003, China
3) State Key Laboratory of Silicon Materials, Department of Materials Science and Engineering, Zhejiang University, Hangzhou 310027, China
(Received: 24 August 2021; revised: 1 November 2021; accepted: 2 November 2021)

Abstract: The practical application of magnesium hydride (MgH_2) was seriously limited by its high desorption temperature and slow desorption kinetics. In this study, a bullet-like catalyst based on vanadium related MOFs (MOFs-V) was successfully synthesized and doped with MgH_2 by ball milling to improve its hydrogen storage performance. Microstructure analysis demonstrated that the as-synthesized MOFs was consisted of V_2O_3 with a bullet-like structure. After adding 7wt% MOFs-V, the initial desorption temperature of MgH_2 was reduced from 340.0 to 190.6°C. Besides, the MgH_2+7wt%MOFs-V composite released 6.4wt% H_2 within 5 min at 300°C. Hydrogen uptake was started at 60°C under 3200 kPa hydrogen pressure for the 7wt% MOFs-V containing sample. The desorption and absorption apparent activity energies of the MgH_2+7wt%MOFs-V composite were calculated to be (98.4 ± 2.9) and (30.3 ± 2.1) kJ·mol^{-1}, much lower than (157.5 ± 3.3) and (78.2 ± 3.4) kJ·mol^{-1} for the as-prepared MgH_2. The MgH_2+7wt%MOFs-V composite exhibited superior cyclic property. During the 20 cycles isothermal dehydrogenation and hydrogenation experiments, the hydrogen storage capacity stayed almost unchanged. X-ray diffraction (XRD) and X-ray photoelectron spectrometer (XPS) measurements confirmed the presence of metallic vanadium in the MgH_2+7wt%MOFs-V composite, which served as catalytic unit to markedly improve the hydrogen storage properties of Mg/MgH_2 system.

Keywords: hydrogen storage; magnesium hydrides; vanadium based MOFs; catalytic mechanism

1. Introduction

Hydrogen has been widely regarded as a renewable energy source due to its higher energy density, rich calorific value of combustion, and no pollution to the environment [1–4]. However, the realization of safe storage and the transport of hydrogen are important factors for developing hydrogen energy economically. Solid state hydrogen storage, which has high hydrogen storage density and excellent security, is promising to fulfill the task of hydrogen transportation [5–7]. In the past decades, many hydrogen storage materials have been extensively researched [8–12]. Lately, MgH_2 was regarded as one of the most potential materials, because MgH_2 possessed superior reversibility, low cost, and high hydrogen storage capacity of 7.6wt%. Nevertheless, the onset desorption temperature of MgH_2 is approximately 340°C and the absorption/desorption kinetics is quite slow, which seriously restrict its practical application [13–16].

To solve these disadvantages of MgH_2, extensive attempts have been devoted, such as alloying with corresponding metallic elements [17–19], nanostructuring [19–21], and catalysts doping [22–26]. Previous studies have proved that introducing catalysts into MgH_2 was a feasible method to enhance the hydrogen storage properties of MgH_2. Particularly, transition metals (Fe, V, Co, Zr, Mn, etc.) and their compounds exhibited outstanding catalytic effect towards MgH_2 [27–30]. Liang *et al.* [31] in 1999 investigated the sorption properties of MgH_2 with different catalysts (Ti, V, Mn, Fe, Ni) and they found V possessed better catalytic effect for the dehydrogenation compared with Ti, Mn, Fe, and Ni. Then they studied the MgH_2–V system and found the MgH_2–5at%V composite could fully release H_2 within 35 min at 235°C [32]. Rizo-Acosta *et al.* [33] examined the catalytic function of Y, Ti, V, Sc, Zr, and Nb on Mg/MgH_2 system, and the desorption kinetics is list as follows: V > Nb > Zr > Ti > Sc > Y. In addition, da Conceição *et al.* [34] compared the effect of VC, VCl_3, and V catalysts on MgH_2. The results revealed the 5wt% VCl_3 containing sample exhibited faster hydrogenation kinetics, it could take up 6wt% H_2 at 350°C in the first 7.5 min. Our previous work [35] synthesized a two-dimensional vanadium nanosheets (V_{NS}) and a remarkable catalytic action on accelerating the hydrogen storage kinetics

*These authors contributed equally to this work.
✉ Corresponding author: Liuting Zhang E-mail: zhanglt89@just.edu.cn

of MgH_2 was evidenced. The initial dehydrogenation temperature of MgH_2+7wt%V_{NS} composite was dropped to 187.2°C, 154°C lower than as-prepared MgH_2. However, the cycling property of the MgH_2+7wt%V_{NS} composite was dissatisfactory. During the first dehydrogenation experiment, the MgH_2+7wt%V_{NS} composite released 6.32wt% hydrogen, unfortunately, only 5.92wt% hydrogen was discharged from the MgH_2+7wt%V_{NS} composite after 20 cycles.

Recently, MOFs materials have become a research hot spot as they have higher specific surface areas, low density, and various framework structures [36–38]. In addition, MOFs materials are also considered as a kind of potential hydrogen storage material due to its special pore structure. Wang *et al.* [39] studied the MgNb/ZIF-67 composite for hydrogen storage and found the dehydrogenation capacity was 4.66wt% in the first cycle and increased to 5.07wt% at the 24th cycle. Wang *et al.* [40] synthesized a nano-V_2O_3@C by a facile hydrothermal synthesis process and demonstrated that the MgH_2+9wt%nano-V_2O_3@C composite began to discharge H_2 at 215°C and released 6.4wt% H_2 within 20 min at 275°C.

With above encouraging results and our previous research on MgH_2+V_{NS} composite, a bullet-like catalyst based on vanadium related MOFs was successfully prepared to comprehensively improve the hydrogen storage property of MgH_2 in this work. The catalytic effect of the synthesized MOFs-V towards the desorption/absorption reactions of MgH_2 was systematically tested. Based on the evidence of microstructure and the evaluation of hydrogen storage property, the catalytic mechanism was discussed in detail.

2. Experimental

2.1. Synthesis of vanadium-based MOFs

Vanadium-based MOFs with a bullet structure was synthesized by a facile hydrothermal reaction and calcination. Firstly, 0.652 g vanadium sulfate oxide hydrate ($VOSO_4$, Alfa, purity 99.9%) and 0.664 g p-Phthalic acid (Alfa, purity 98%) were dissolved in 45 mL dimethylformamide (DMF, Alfa, purity 99.8%) solution and violently stirred for 45 min in a 100 mL stainless steel autoclave. The autoclave was put into a stove and heated to 160°C for 36 h. The mixtures were washed 8 times with methanol and dried in vacuum at 180°C for 24 h. Finally, vanadium-based MOFs materials were obtained after been calcined at 700°C for 5 h in a N_2 atmosphere, as shown in Fig. 1.

2.2. Preparation of MgH_2+MOFs-V composites

First of all, 6 g commercial Mg powder (Aladdin, 100–200 mesh (75–150 μm), purity 99.99%) were packed and sealed into the reactor, then the Mg powder were hydrogenated under the hydrogen pressure of 6.5 MPa with the temperature of 380°C for 2 h. The hydrogenated Mg powder were collected and conducted to mechanical ball milling with a speed of 450 r/min for 5 h. Finally, MgH_2 was obtained after been hydrogenated under 6.5 MPa H_2 pressure at 380°C for 2 h. In order to get MgH_2+MOFs-V composite, MOFs-V particles were ball milled with MgH_2 under argon atmosphere. To systematically examine the catalytic effectiveness of MOFs-V, various amounts of MOFs-V particles were adopted, denoted as MgH_2+5wt%MOFs-V, MgH_2+7wt% MOFs-V, and MgH_2+9wt%MOFs-V, respectively.

2.3. Sample characterization

The as-prepared samples were tested by X-ray diffraction (XRD) measurement using an X'Pert Pro X-ray diffractometer (PANalytical, the Netherlands) with Cu K_α radiation at 40 kV, 40 mA. The scanning rate was $1°\cdot min^{-1}$. X-ray photoelectron spectrometer (XPS) was conducted to explore the binding energy of related elements. Moreover, the microstructure characterization and elemental analysis of the samples were carried out by scanning electron microscopy

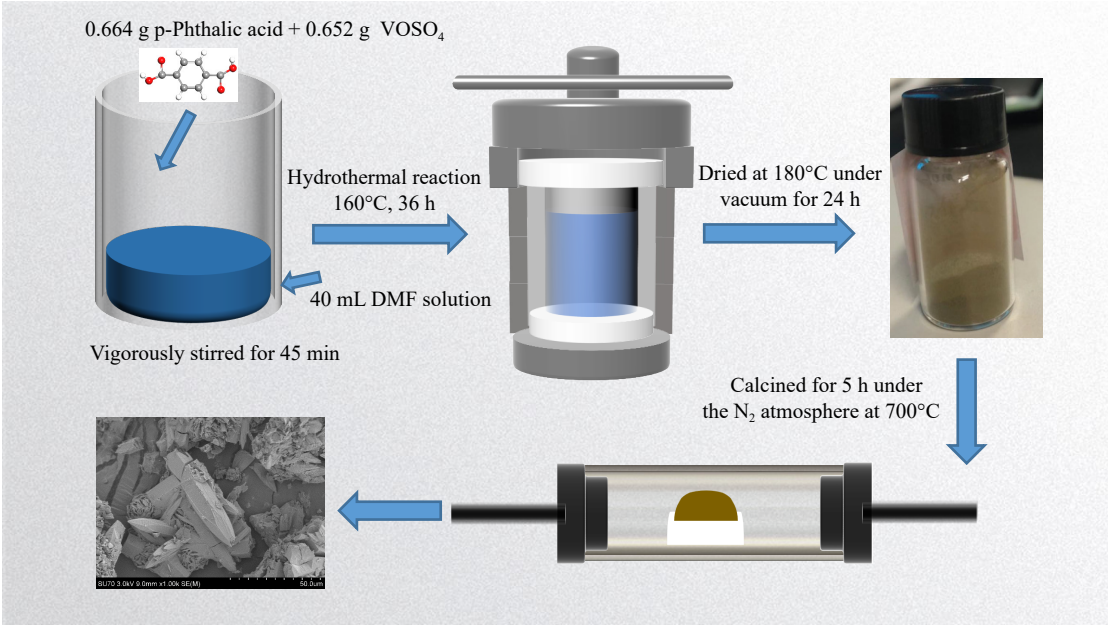

Fig. 1. Schematic diagram of the preparation of MOFs-V.

(SEM) and transmission electron microscope (TEM, Tecnai G2 F30 operated at 300 kV) with an energy dispersive spectrometry (EDS).

The dehydrogenation and rehydrogenation experiments were conducted in a pressure-composition-temperature (PCT) apparatus (Sievert type). Approximately 130 mg samples were packed in a steel tube in each test. The samples were heated to 450°C for the non-isothermal dehydrogenation experiments. The fully dehydrogenated samples were heated to 380°C under 3.2 MPa H_2 for non-isothermal hydrogen absorption experiments. For cycling tests, samples were hydrogenated under 3.2 MPa hydrogen pressure and desorbed in vacuum for 20 times at 300°C, respectively. Differential scanning calorimetry (DSC, STA449F3 Jupiter) measurement was conducted in a Netzsh STA449F3 equipment under high purity Ar atmosphere and the heating rate was 5, 8, 10, and 12 $K \cdot min^{-1}$, respectively.

3. Results and discussion

3.1. Characterization of synthesized MOFs-V

Fig. 2(a) denotes the XRD profile of synthesized MOFs-V. Apparently, the XRD peaks for MOFs-V are in great agreement with the PDF card of V_2O_3 (PDF#78-7574: V_2O_3 and PDF#74-0325: V_2O_3). The refined XRD result indicates the content of PDF#78-7574: V_2O_3 and PDF#74-0325: V_2O_3 in as-synthesized MOFs-V is 70.8wt% and 29.2wt%, respectively. XPS test was carried out to further verify the chemical state of vanadium in MOFs-V, as shown in Fig. 2(b). From the XPS spectra of O 1s and V 2p, four peaks at 530.3, 524.1, 516.8, and 532.4 eV could be observed. In addition, the peaks at 524.1 and 516.8 eV were related to V–O bond. The peaks at 532.4 and 530.3 eV came from O–H and O^{2-} bonds. Based on the XRD and XPS results, it could be concluded V_2O_3 containing MOFs materials were successfully synthesized. TEM and SEM tests were adopted to reveal the micromorphology of as-synthesized MOFs-V. SEM image presents a bullet-like structure with a height of 62 um and width of 13 um in Fig. 2(c). Besides, TEM image (Fig. 2(d)) also verifies the as-synthesized MOFs-V materials have a bullet-like structure.

3.2. Catalytic effect of MOFs-V towards the dehydrogenation performance of MgH_2

The bullet-like MOFs-V was mixed with MgH_2 to study the catalytic effectiveness. Fig. 3(a) denotes the heating-up dehydrogenation curves of the MgH_2+*x*wt%MOFs-V (*x* = 0, 5, 7, and 9) composite. It was observed as-prepared MgH_2 began to release H_2 at 340.0°C and the final desorption capacity was 7.3wt%. Apparently, after adding MOFs-V, the initial desorption temperature of MgH_2 was significantly reduced. The 5wt% MOFs-V containing sample began to release H_2 at 199.8°C, which was 140.2°C lower than that of additive-free MgH_2. When the temperature was increased to 328.5°C, the MgH_2+5wt%MOFs-V composite could fully release 6.9wt% hydrogen. Increasing the doping amount of MOFs-V to 7wt% and 9wt%, the onset desorption temperature was further decreased to 190.6 and 186.1°C, respectively.

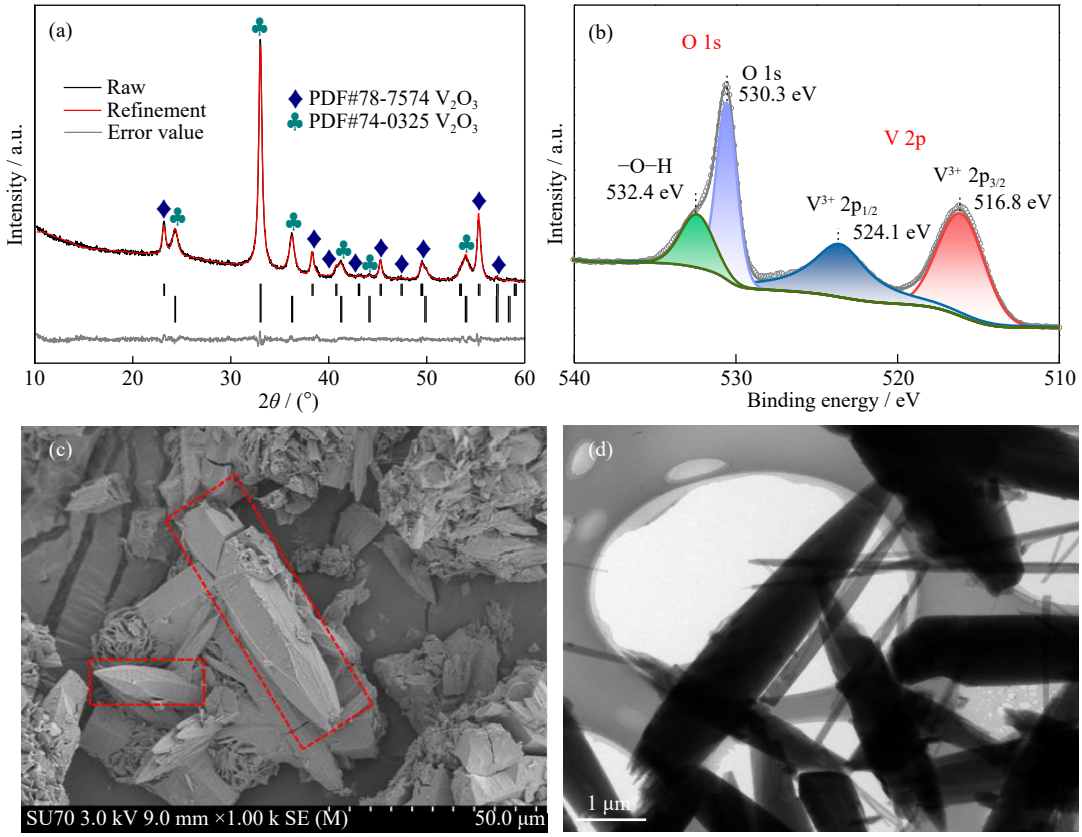

Fig. 2. Characterizations of as-prepared MOFs-V: (a) XRD profile; (b) XPS spectra; (c, d) SEM and TEM images.

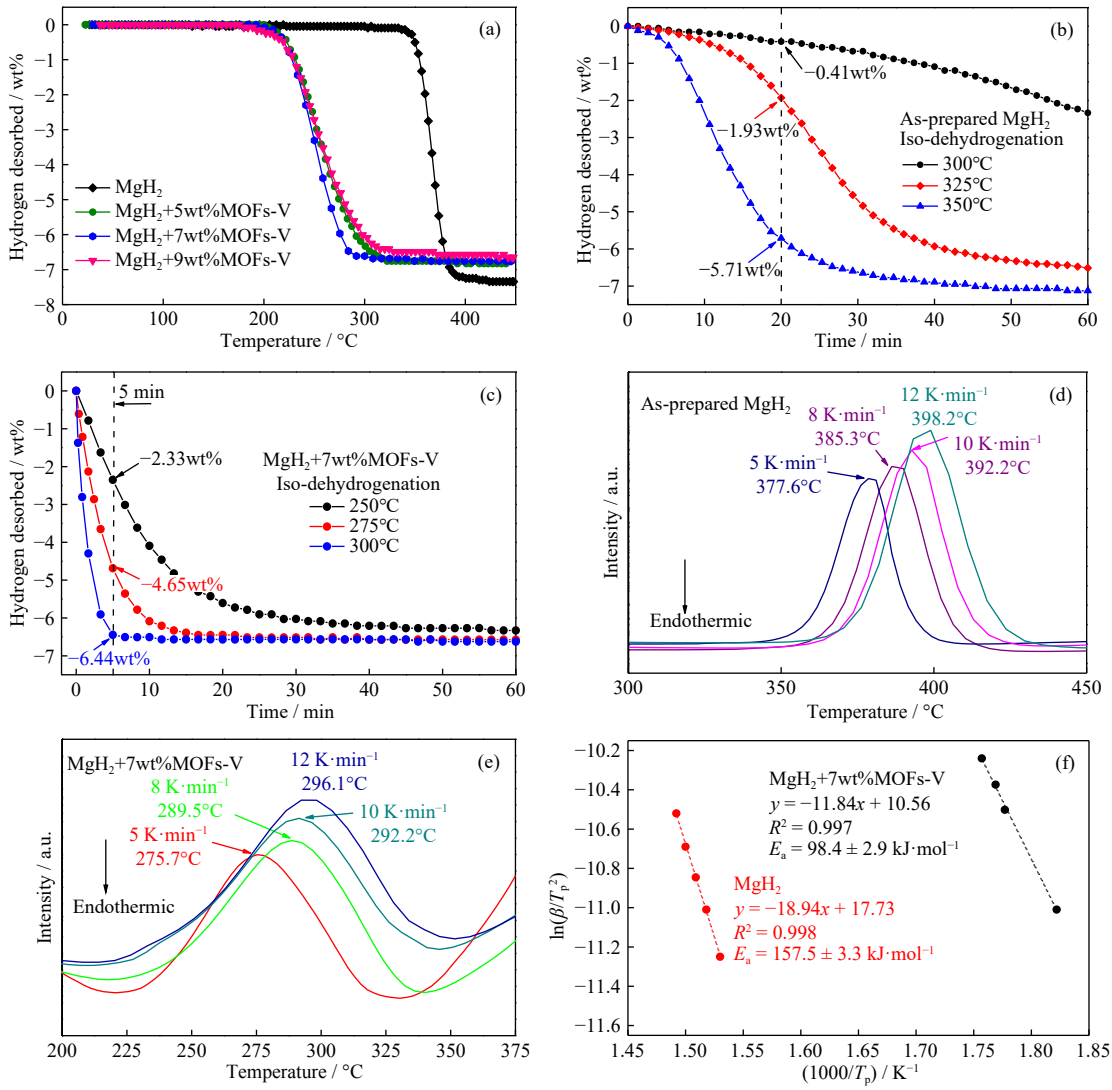

Fig. 3. (a) Non-isothermal desorption curves of MgH_2+*x*wt%MOFs-V (*x* = 0, 5, 7, 9). (b) Isothermal dehydrogenation curves for MgH_2 at 300, 325, 350°C. (c) Isothermal dehydrogenation curves for MgH_2+7wt%MOFs-V composite at 250, 275, 300°C. DSC curves of (d) as-prepared MgH_2 and (e) MgH_2+7wt%MOFs-V composite. (f) Kissinger's plot of the MgH_2 and MgH_2+7wt%MOFs-V composite.

However, the hydrogen capacity was also successive decreased to 6.8wt% and 6.6wt% for the MgH_2+7wt%MOFs-V composite and MgH_2+9wt%MOFs-V composite. The reason for this phenomenon was that the existence of MOFs-V reduced the available hydrogen storage capacity. Taken both the onset desorption temperature and capacity in consideration, the MgH_2+7wt%MOFs-V composite possessed the optimal dehydrogenation performance compared with MgH_2+5wt%MOFs-V composite and MgH_2+9wt%MOFs-V composite. Therefore, other follow-up experiments were carried out on the MgH_2+7wt%MOFs-V composite. In order to further study the desorption performance, isothermal dehydrogenation experiments were carried out. Fig. 3(b) and (c) denoted the isothermal desorption curves at different temperatures for MgH_2 and the MgH_2+7wt%MOFs-V composite. Fig. 3(b) indicated as-prepared MgH_2 exhibited slow desorption kinetics, only 0.41wt%, 1.93wt%, and 5.71wt% H_2 was released within 20 min at 300, 325, and 350°C, respectively. However, the MgH_2+7wt%MOFs-V composite discharged about 6.44wt% H_2 at 300°C and 4.65wt% H_2 at 275°C in 5 min, as shown in Fig. 3(c). The effect of MOFs-V on desorption kinetic performance for MgH_2 was further investigated by DSC measurement and Kissinger method. Fig. 3(d) and (e) displays the DSC curves with various heating rates (5, 8, 10, and 12 $K \cdot min^{-1}$) for as-prepared MgH_2 and MgH_2+7wt%MOFs-V samples. Obviously, after adding MOFs-V to MgH_2, the peak temperatures were shifted to lower temperatures compared with as-prepared MgH_2. For instance, the peak temperature for MgH_2+7wt%MOFs-V composite was 296.6°C when the heating rate was 12 $K \cdot min^{-1}$, however, the peak temperature for as-prepared MgH_2 was 398.2°C under the same condition.

In addition, the apparent activity energy (E_a) for the isothermal desorption experiments was calculated through Kissinger method [41]:

$$\ln\left(\frac{\beta}{T_p^2}\right) = -\frac{E_a}{RT_p} + \ln\left(\frac{AR}{E_a}\right) \quad (1)$$

where T_p is the peak temperature; β represents the heating

rate; A and R mean the pre-exponential factor and gas constant, respectively.

The apparent activity energy of MgH_2+7wt%MOFs-V composite was estimated to be (98.4 ± 2.9) kJ·mol^{-1}, and approximately 38% reduction was achieved compared to (157.5 ± 3.3) kJ·mol^{-1} for the as-prepared MgH_2. In addition, the dehydrogenation apparent activity energy values of different MgH_2+catalyst systems are shown in Table 1. It is proved that MOFs-V is of great help to reduce the dehydrogenation apparent activity energy. The significant decrease in activity energy contributed to the lowered initial dehydrogenation temperatures and accelerated dehydrogenation kinetics of MOFs-V modified MgH_2, as reported above.

To further investigate the hydrogen desorption thermodynamics of MgH_2+7wt%MOFs-V composite, the pressure-composites-temperature measurements were carried out. Fig. 4(a) and (b) displays the PCT curves for MgH_2 and the MgH_2+7wt% MOFs-V composite at various temperatures. It was observed each temperature had a corresponding platform in the PCT curve. For instance, the desorption flat plateau of MgH_2 were 0.23, 0.42, 0.86, and 1.03 MPa for 325, 350, 375, and 400°C shown in Fig. 4(a). As for the MgH_2+7wt%MOFs-V composite, the plateau pressures were determined to be 0.18, 0.24, 0.58, and 0.92 MPa for 300, 325, 350, and 375°C in Fig. 4(b). The decomposition enthalpy ΔH was estimated using the Van't Hoff equation:

$$\ln P = \Delta H/RT - \Delta S/R \quad (2)$$

where P is pressure, ΔS denotes the decomposition entropy, ΔH means the decomposition enthalpy, R is universal gas constant, T represents temperature. The obtained Van't Hoff plot is shown in Fig. 4(c) and (d) for MgH_2 and MgH_2+7wt%MOFs-V composite. The decomposition enthalpy ΔH is determined to be (86.2 ± 6.3) kJ·mol^{-1} for MgH_2 and (84.8 ± 1.9) kJ·mol^{-1} for the MgH_2+7wt%MOFs-V composite. The results suggest that the addition of MOFs-V has negligible effect on thermodynamics property of MgH_2.

3.3. Rehydrogenation performance of MgH_2+7wt% MOFs-V composite

The catalytic action of MOFs-V on hydrogen absorption was also studied. Fig. 5(a) shows the non-isothermal hydro-

Table 1. Dehydrogenation apparent activity energy values of different MgH_2+catalyst systems

Sample	Method for calculating desorption E_a	E_a / (kJ·mol^{-1})	Ref.
MgH_2+7wt%MOFs-V	Kissinger equation	90.1	This work
MgH_2–CuS	Kissinger equation	123.7	[42]
MgH_2–10wt%$CoMoO_4$	Kissinger equation	108.0	[43]
MgH_2–10wt%$LaFeO_3$	Kissinger equation	107.0	[44]
MgH_2@CoS–NBs	Kissinger equation	120.8	[45]
MgH_2–5wt%$K_2Ti_8O_{17}$	Kissinger equation	116.3	[46]
MgH_2–TiN@rGO	Kissinger equation	120.0	[47]
MgH_2+10wt%$SrTiO_3$	Kissinger equation	109.0	[48]

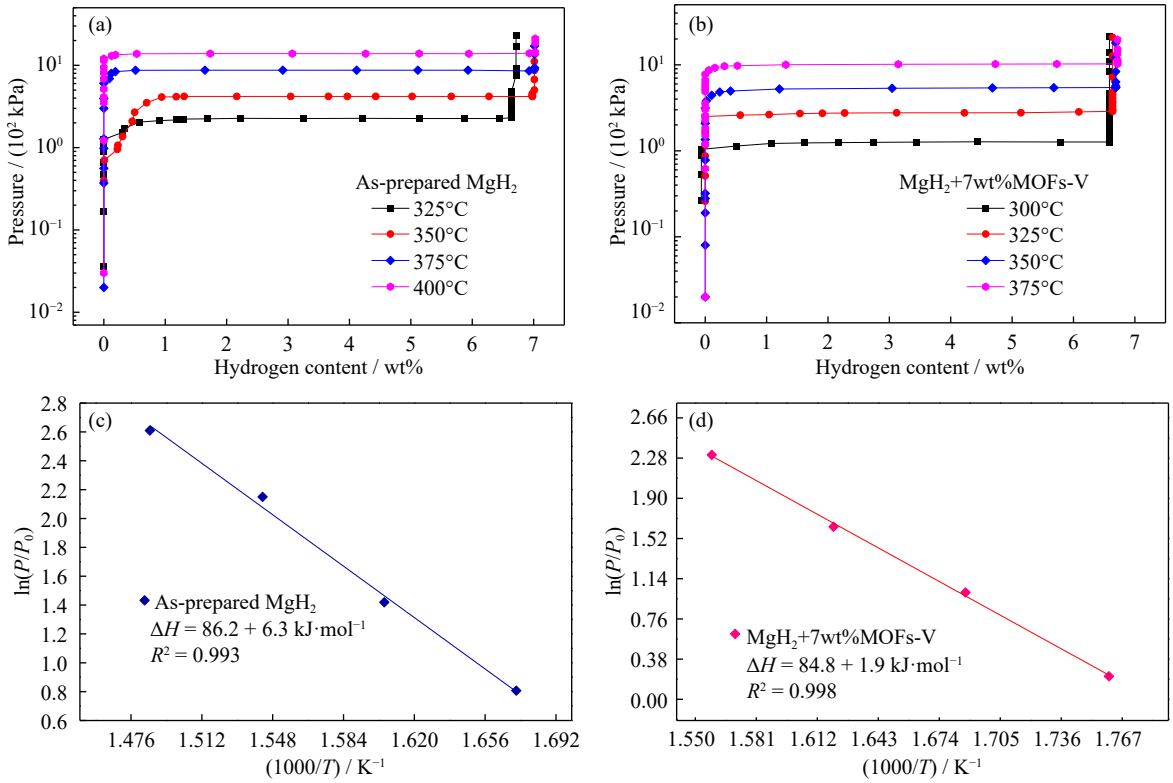

Fig. 4. PCT curves for (a) MgH_2 and (b) MgH_2+7wt%MOFs-V composite at various temperatures. Corresponding Vant't Hoff plot of (c) MgH_2 and (d) MgH_2+7wt%MOFs-V composite.

gen absorption curves for the fully dehydrogenated MgH_2 and MgH_2+7wt%MOFs-V samples. The fully dehydrogenated MgH_2 began to uptake H_2 at about 181°C and hydrogen absorption finished at 399°C with 7.3wt% hydrogen capacity. The 7wt% MOFs-V containing sample started absorbing hydrogen even at 60°C and 6.7wt% hydrogen was charged when the temperature was heated to 217°C, 3 times higher than 2.0wt% of fully dehydrogenated MgH_2. In addition, isothermal rehydrogennation experiments were carried out, shown in Fig. 5(b) and (c). It can be clearly seen that the hydrogen absorption kinetics was accelerated with rising temperatures and addition of MOFs-V. The fully dehydrogenated MgH_2 only absorbed 1.04wt%, 2.74wt%, and 4.96wt% H_2 at 200, 225, and 250°C in the first 10 min, respectively. For the 7wt% MOFs-V containing sample, 2.34wt% H_2 was absorbed within the first 10 min even at low temperature of 100°C. At 125 and 150°C, approximately 3.79wt% and 4.88wt% H_2 were taken up by the 7wt% MOFs-V containing sample in the first 10 min. Besides, in order to obtain an insight into the improvement of hydrogen absorption kinetics of the samples, the isothermal absorption curves of the as-prepared MgH_2 and the MgH_2+7wt%MOFs-V composite at different temperatures were fitted using the Johnson–Mehl–Avrami–Kolmogorov (JMAK) equation [49]:

$$\ln[-\ln(1-\alpha)] = n\ln k + \ln t \tag{3}$$

where a is the extent of reaction; t denotes the reaction duration; n means the Avrami exponent; k represents the rate constant. Subsequently, the E_a for hydrogenation reaction could be estimated by Arrhenius equation:

$$k = A\exp\left(-\frac{E_a}{RT}\right) \tag{4}$$

where T represents the isothermal hydrogen absorption temperature and A means the pre-exponential factor and R is universal gas constant. In this work, the hydrogen absorption activation energy values of the as-prepared MgH_2 and the MgH_2+7wt%MOFs-V composite were calculated to be (78.2 ± 3.4) and (30.3 ± 2.1) kJ·mol^{-1}, respectively (Fig. 5(d)). Obviously, with the addition of MOFs-V, the apparent activation energy for the hydrogen absorption of MgH_2 was significantly reduced, which was directly responsible for the enhancement in the hydrogen absorption kinetics of MgH_2.

3.4. Cycling feature of MgH_2+7wt%MOFs-V composite

Cycling performance was considered as an indispensable factor for the practical use of hydrogen storage materials. Therefore, the cyclic property was tested for the MgH_2+7wt% MOFs-V composite in an isothermal mode. Fig. 6(a) and (b) displays the curves of isothermal dehydrogenation (static vacuum) and rehydrogenation (3.2 MPa H_2 pressure) in the first 20 cycles at 300°C, respectively. The results denoted the MgH_2+7wt%MOFs-V composite released 6.44wt% H_2 in the first cycle and 6.40wt% H_2 was still discharged for the tenth isothermal dehydrogenation experiment. In the 20th cycle, MgH_2+7wt%MOFs-V composite desorbed 6.37wt% H_2, maintain 98.9% hydrogen capacity compared with the first cycle (Fig. 6). For the hydrogen absorption, MgH_2+7wt% MOFs-V composite absorbed 6.44wt% hydrogen in the first cycle and 6.37wt% hydrogen was charged into the 7wt% MOFs-V containing sample in the 20th cycle. Table 2 sum-

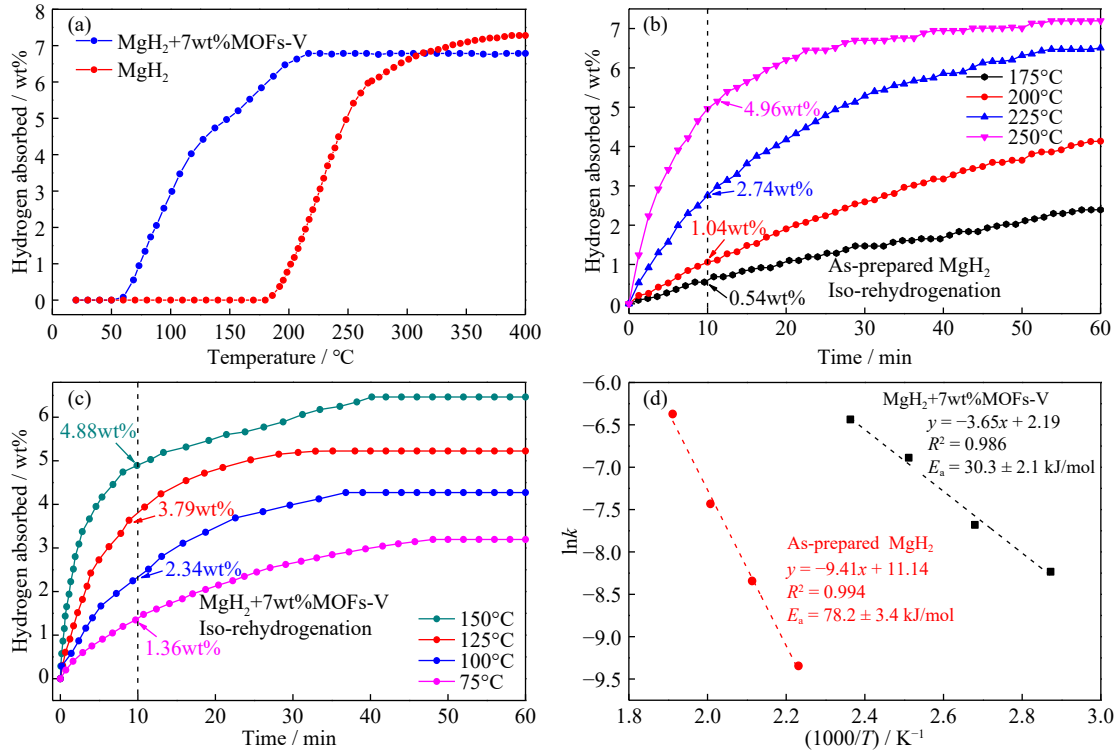

Fig. 5. (a) Hydrogen absorption curves with different temperatures for MgH_2 and MgH_2+7wt%MOFs-V composite. Isothermal rehydrogenation curves for (b) MgH_2 and (c) MgH_2+7wt%MOFs-V composite. (d) Fitted Arrhenius curves for MgH_2 and MgH_2+7wt%MOFs-V composite.

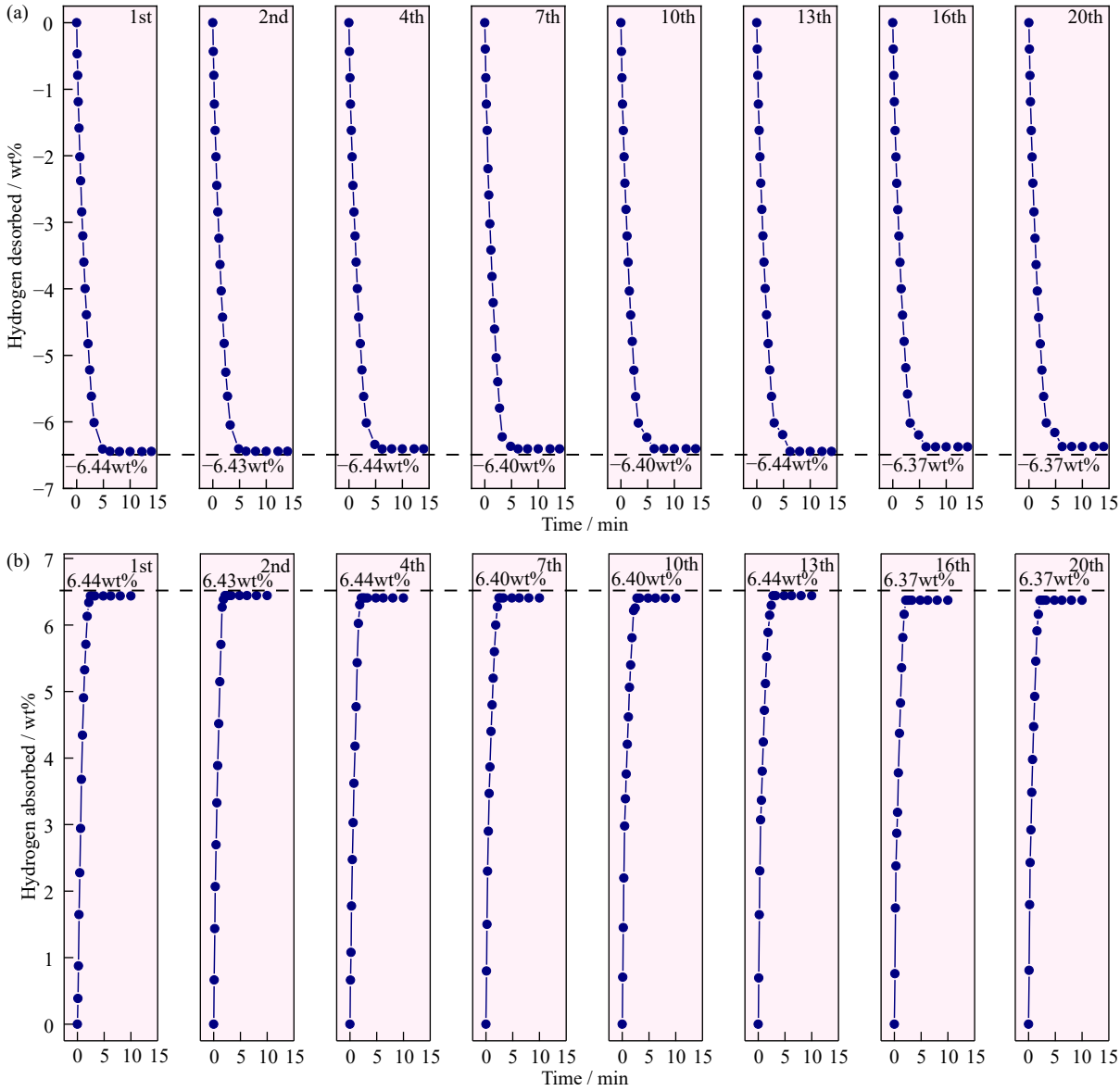

Fig. 6. Cycling hydrogen desorption (a) and absorption (b) curves of MgH_2+7wt%MOFs-V composite for 20 times at 300°C.

marizes the hydrogen capacity of MgH_2 modified by different catalysts. Compared with other MgH_2 systems, the MgH_2+7wt%MOFs-V composite presents superior cycling stability.

3.5. Catalytic mechanism of MOFs-V on MgH_2

To explore the catalytic mechanism of MOFs-V on MgH_2, XRD experiment was carried out. Fig. 7(a) displays the XRD profiles of MgH_2+7wt%MOFs-V at different stages. Apparently, the peaks of ball milled MgH_2+7wt%MOFs-V and rehydrogenated MgH_2+7wt%MOFs-V samples are conformed to the PDF card of MgH_2. For the dehydrogenated MgH_2+7wt%MOFs sample, all of the MgH_2 phase was converted to metallic Mg phase. Interesting, a weak peak representing metallic vanadium can be detected at 42.2° for the above samples, indicative of the reduction reaction between MOFs-V and MgH_2 during the dehydrogenation and rehydrogenation process. In order to further explore the evaluation of MOFs-V, XPS measurements were conducted. Clearly,

Table 2. Dehydrogenation capacity for different catalysts doped MgH_2 wt%

Sample	First cycle	Last cycle	Ref.
MgH_2–Co/Pd@B–CNTS	6.45	6.45	[50]
MgH_2+Ni@Ti–MX	5.35	5.35	[51]
MgH_2+$TiNb_2O_7$	6.75	6.50	[52]
MgH_2+V_2C/Ti_3C_2	6.30	6.30	[53]
MgH_2–8wt%Ni/C	6.5	6.7	[54]
MgH_2–10wt%TiO_2@C	6.2	6.0	[55]
MgH_2–TiO_2 SCNPs/AC	6.5	6.2	[56]
MgH_2–5wt%NiS_2	6.15	6.10	[57]
MgH_2+MOFs-V	6.44	6.37	This work

the peaks of MgO could be detected in the ball milled and dehydrogenated samples (Fig. 7(b)), indicting the reaction between MgH_2 and MOFs-V occurred during the ball milling process. Besides, XPS examination confirmed the presence of V^{0+} and V^{3+} for the as-milled and dehydrogenated samples in Fig. 7(c) and (d) and the content of V^{0+} for the dehydro-

genated sample is higher than that of the as-milled sample. During the ball milling process, there was a possibility that the energy produced by ball hitting would help V_2O_3 react MgH_2 to form metallic vanadium. In the dehydrogenation process, due to the high temperature, it was easier for V_2O_3 to be reduced to metallic vanadium. Combining the XRD and XPS results, the gradual conversion of MOFs-V to metallic vanadium was further verified. Our previous work has evidenced that metallic vanadium possessed excellent catalytic effect for hydrogen storage in MgH_2 [35]. In this case, the V_2O_3 in MOFs-V gradually reacted with MgH_2 to form metallic vanadium, which served as active catalyst for improving the hydrogen storage property of MgH_2.

Furthermore, morphology and element distribution of MgH_2+7wt%MOFs-V composite were confirmed by TEM and EDS measurements. Fig. 8(a–c) indicates the MgH_2+

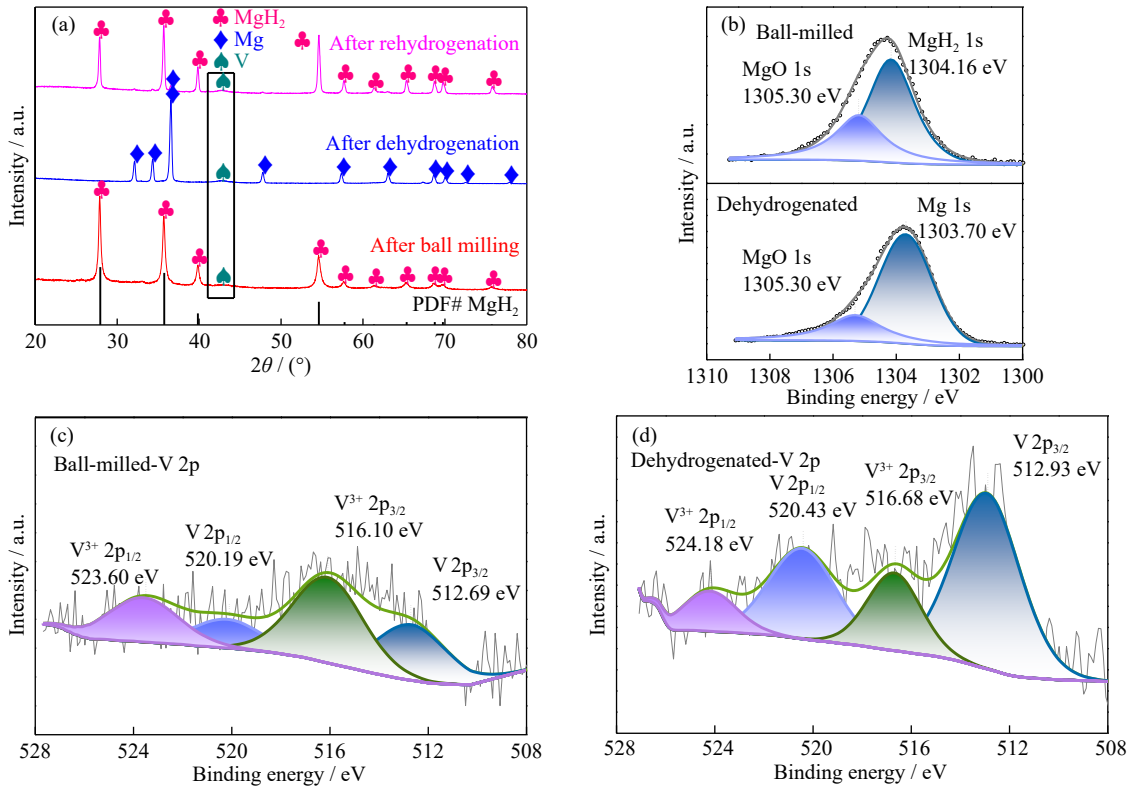

Fig. 7. (a) XRD patterns of the MgH_2+7wt%MOFs-V composite at different stages. XPS curves of ball-milled and dehydrogenated MgH_2+7wt%MOFs-V samples: (b) Mg 1s and (c, d) V 2p.

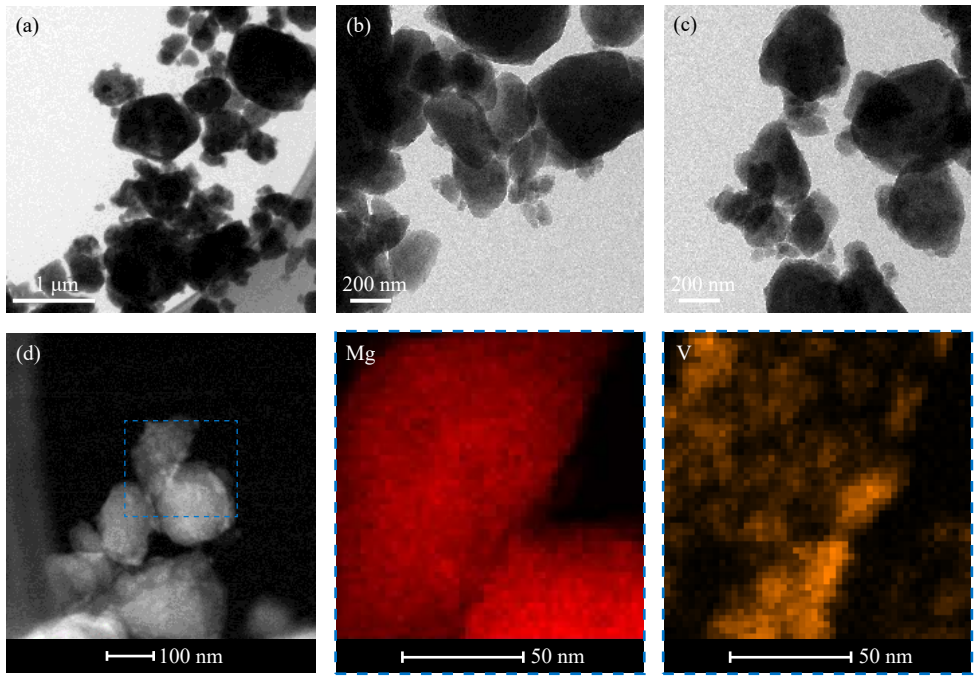

Fig. 8. TEM images (a–c) and corresponding EDS mapping (d) of MgH_2+7wt%MOFs-V composite after 20 cycles.

7wt%MOFs-V composite is consisted of particles with size around 350 nm. It is well known that nanostructured materials would reduce the diffusion distance for hydrogen uptake and desorbed, resulting in a promoted hydrogen kinetics in MgH_2 [58–60]. Moreover, the EDS mapping results (Fig. 8(d)) indicated that vanadium was uniformly dispersed on the surface of MgH_2, which helped to enhance the firm contact between catalysts with MgH_2, thus creating numerous hydrogen channels to accelerate the hydrogen diffusion rate during hydrogenation and dehydrogenation. In addition, MOFs materials could further improve the activity of metal catalysts [61], meanwhile, the carbon in MOFs materials prevented MgH_2 particles from aggregation and growing, thus maintaining the cycle stability for hydrogen storage [54]. In a word, MOFs supported transition metal materials have shown excellent catalytic action for MgH_2, which may be helpful for the further design and preparation of efficient catalysts for hydrogen storage and other energy-related fields.

4. Conclusion

In this work, bullet-like MOFs-V was successfully prepared via a facile hydrothermal reaction and high-temperature calcination. After adding 7wt% MOFs-V, the MgH_2+ 7wt%MOFs-V composite started to release H_2 at 190.6°C, and it could fully release H_2 within 5 min at 300°C. Moreover, the hydrogen absorption began at 60°C, and when the temperature was heated to 150°C, 4.88wt% H_2 was charged into the fully dehydrogenated sample in the first 10 min, while only 1.04wt% H_2 was absorbed by the as-prepared MgH_2 even at 200°C. For the cycling performance of 7wt% MOFs-V containing sample, 98.9% hydrogen capacity was remained compared to the first dehydrogenation capacity. Microstructure analysis revealed that MOFs-V was reduced to metallic vanadium and served as catalytic union during dehydrogenation and rehydrogenation process. The combining effect of MOFs and transition metals manifested enhanced catalytic action for MgH_2, which provides an insight into the improvement of hydrogen storage property of MgH_2 by introducing MOFs as an efficient modification agent.

Acknowledgements

This work was financially supported by the National Natural Science Foundation of China (No. 51801078) and the Natural Science Foundation of Jiangsu Province (No. BK20180986).

Conflict of Interest

The authors declared that they have no conflicts of interest in this work.

References

[1] L. Schlapbach and A. Züttel, Hydrogen-storage materials for mobile applications, *Nature*, 414(2001), No. 6861, p. 353.
[2] Q. Li, X. Lin, Q. Luo, *et al*., Kinetics of the hydrogen absorption and desorption processes of hydrogen storage alloys: A review, *Int. J. Miner. Metall. Mater.*, 29(2022), No. 1, p. 32.
[3] M. Chen, Y.H. Pu, Z.Y. Li, *et al*., Synergy between metallic components of MoNi alloy for catalyzing highly efficient hydrogen storage of MgH_2, *Nano Res.*, 13(2020), No. 8, p. 2063.
[4] F.M. Nyahuma, L.T. Zhang, M.C. Song, *et al*., Significantly improved hydrogen storage behaviors of MgH_2 with Nb nanocatalyst, *Int. J. Miner. Metall. Mater.*, 29(2022), No. 9, p. 1788.
[5] X.S. Liu, H.Z. Liu, N. Qiu, *et al*., Cycling hydrogen desorption properties and microstructures of MgH_2–AlH_3–NbF_5 hydrogen storage materials, *Rare Met.*, 40(2021), No. 4, p. 1003.
[6] J.Z. Song, Z.Y. Zhao, X. Zhao, R.D. Fu, and S.M. Han, Hydrogen storage properties of MgH_2 co-catalyzed by LaH_3 and NbH, *Int. J. Miner. Metall. Mater.*, 24(2017), No. 10, p. 1183.
[7] M. Ismail, M.S. Yahya, N.A. Sazelee, *et al*., The effect of K_2SiF_6 on the MgH_2 hydrogen storage properties, *J. Magnes. Alloys*, 8(2020), No. 3, p. 832.
[8] Q.Q. Kong, H.H. Zhang, Z.L. Yuan, *et al*., Hamamelis-like $K_2Ti_6O_{13}$ synthesized by alkali treatment of Ti_3C_2 MXene: Catalysis for hydrogen storage in MgH_2, *ACS Sustainable Chem. Eng.*, 8(2020), No. 12, p. 4755.
[9] Q. Li, K.C. Chou, Q. Lin, L.J. Jiang, and F. Zhan, Hydrogen absorption and desorption kinetics of Ag–Mg–Ni alloys, *Int. J. Hydrogen Energy*, 29(2004), No. 8, p. 843.
[10] Z.Y. Li, S.L. Li, Z.M. Yuan, Y.H. Zhang, and Y. Qi, Microstructure, hydrogen storage thermodynamics and kinetics of $La_5Mg_{95-x}Ni_x$ (x = 5, 10, 15) alloys, *Trans. Nonferrous Met. Soc. China*, 29(2019), No. 5, p. 1057.
[11] X.P. Ren, F.F. Zhang, Q.M. Guo, H.L. Hou, and Y.Q. Wang, Hydrogen absorption behavior of TA15 alloy, *Int. J. Miner. Metall. Mater.*, 18(2011), No. 2, p. 210.
[12] M.J. Liu, S.C. Zhao, X.Z. Xiao, *et al*., Novel 1D carbon nanotubes uniformly wrapped nanoscale MgH_2 for efficient hydrogen storage cycling performances with extreme high gravimetric and volumetric capacities, *Nano Energy*, 61(2019), p. 540.
[13] Y.F. Liu, H.F. Du, X. Zhang, *et al*., Superior catalytic activity derived from a two-dimensional Ti_3C_2 precursor towards the hydrogen storage reaction of magnesium hydride, *Chem. Commun.*, 52(2016), No. 4, p. 705.
[14] C. Lu, J.X. Zou, X.Y. Shi, X.Q. Zeng, and W.J. Ding, Synthesis and hydrogen storage properties of core–shell structured binary Mg@Ti and ternary Mg@Ti@Ni composites, *Int. J. Hydrogen Energy*, 42(2017), No. 4, p. 2239.
[15] X. Lu, L.T. Zhang, H.J. Yu, *et al*., Achieving superior hydrogen storage properties of MgH_2 by the effect of TiFe and carbon nanotubes, *Chem. Eng. J.*, 422(2021), art. No. 130101.
[16] L.Z. Ouyang, F. Liu, H. Wang, *et al*., Magnesium-based hydrogen storage compounds: A review, *J. Alloys Compd.*, 832(2020), art. No. 154865.
[17] J.T. Hu, J.J. Zhang, H.Y. Xiao, *et al*., A first-principles study of hydrogen storage of high entropy alloy TiZrVMoNb, *Int. J. Hydrogen Energy*, 46(2021), No. 40, p. 21050.
[18] Y.H. Zhang, W. Zhang, Z.M. Yuan, *et al*., Hydrogen storage performances of as-milled $REMg_{11}Ni$ (RE = Y, Sm) alloys catalyzed by MoS_2, *Trans. Nonferrous Met. Soc. China*, 28(2018), No. 9, p. 1828.
[19] W.L. Mi, Z.S. Liu, T. Kimura, A. Kamegawa, and H.L. Wang, Crystal structure and hydrogen storage properties of (La, Ce)$Ni_{5-x}M_x$ (M = Al, Fe, or Co) alloys, *Int. J. Miner. Metall. Mater.*, 26(2019), No. 1, p. 108.
[20] C.Q. Zhou, Y.Y. Peng, and Q.G. Zhang, Growth kinetics of MgH_2 nanocrystallites prepared by ball milling, *J. Mater. Sci. Technol.*, 50(2020), p. 178.
[21] T.Z. Si, Y. Cao, Q.G. Zhang, *et al*., Enhanced hydrogen storage properties of a Mg–Ag alloy with solid dissolution of indium: A comparative study, *J. Mater. Chem. A*, 3(2015), No. 16, p. 8581.
[22] M.G. Verón, H. Troiani, and F.C. Gennari, Synergetic effect of Co and carbon nanotubes on MgH_2 sorption properties, *Carbon*, 49(2011), No. 7, p. 2413.

[23] B. Wang, D.Y. Ong, Y.H. Li, *et al*., Stereo-controlled anti-hydromagnesiation of aryl alkynes by magnesium hydrides, *Chem. Sci.*, 11(2020), No. 20, p. 5267.
[24] K. Wang, X. Zhang, Y.F. Liu, *et al*., Graphene-induced growth of N-doped niobium pentaoxide nanorods with high catalytic activity for hydrogen storage in MgH_2, *Chem. Eng. J.*, 406(2021), art. No. 126831.
[25] C.C. Xu, X.Z. Xiao, J. Shao, *et al*., Effects of Ti-based additives on Mg_2FeH_6 dehydrogenation properties, *Trans. Nonferrous Met. Soc. China*, 26(2016), No. 3, p. 791.
[26] Y. Wang, C.H. An, Y.J. Wang, *et al*., Core–shell Co@C catalyzed MgH_2: Enhanced dehydrogenation properties and its catalytic mechanism, *J. Mater. Chem. A*, 2(2014), No. 38, p. 16285.
[27] Z.Y. Wang, X.L. Zhang, Z.H. Ren, *et al., In situ* formed ultrafine NbTi nanocrystals from a NbTiC solid-solution MXene for hydrogen storage in MgH_2, *J. Mater. Chem. A*, 7(2019), No. 23, p. 14244.
[28] L.T. Zhang, Z.L. Cai, Z.D. Yao, *et al*., A striking catalytic effect of facile synthesized $ZrMn_2$ nanoparticles on the de/rehydrogenation properties of MgH_2, *J. Mater. Chem. A*, 7(2019), No. 10, p. 5626.
[29] N.H. Yan, X. Lu, Z.Y. Lu, *et al.*, Enhanced hydrogen storage properties of Mg by the synergistic effect of grain refinement and $NiTiO_3$ nanoparticles, *J. Magnes. Alloys*, 2021. DOI: 10.1016/j.jma.2021.03.014
[30] M.C. Song, L.T.Zhang, J.G. Zheng, Z.D. Yu, and S.N. Wang, Constructing graphene nanosheet-supported FeOOH nanodots for hydrogen storage of MgH_2, *Int. J. Miner. Metall. Mater.*, 29(2022), No. 7, p. 1464.
[31] G. Liang, J. Huot, S. Boily, A. van Neste, and R. Schulz, Catalytic effect of transition metals on hydrogen sorption in nanocrystalline ball milled MgH_2–Tm (Tm = Ti, V, Mn, Fe and Ni) systems, *J. Alloys Compd.*, 292(1999), No. 1-2, p. 247.
[32] G. Liang, J. Huot, S. Boily, A. van Neste, and R. Schulz, Hydrogen storage properties of the mechanically milled MgH_2–V nanocomposite, *J. Alloys Compd.*, 291(1999), No. 1-2, p. 295.
[33] P. Rizo-Acosta, F. Cuevas, and M. Latroche, Hydrides of early transition metals as catalysts and grain growth inhibitors for enhanced reversible hydrogen storage in nanostructured magnesium, *J. Mater. Chem. A*, 7(2019), No. 40, p. 23064.
[34] M.O.T. da Conceição, M.C. Brum, and D.S. dos Santos, The effect of V, VCl_3 and VC catalysts on the MgH_2 hydrogen sorption properties, *J. Alloys Compd.*, 586(2014), p. S101.
[35] Z.Y. Lu, H.J. Yu, X. Lu, *et al*., Two-dimensional vanadium nanosheets as a remarkably effective catalyst for hydrogen storage in MgH_2, *Rare Met.*, 40(2021), No. 11, p. 3195.
[36] L.T. Zhang, Z.L. Cai, X.Q. Zhu, *et al*., Two-dimensional ZrCo nanosheets as highly effective catalyst for hydrogen storage in MgH_2, *J. Alloys Compd.*, 805(2019), p. 295.
[37] L.T. Zhang, L.X. Chen, X.L. Fan, *et al*., Enhanced hydrogen storage properties of MgH_2 with numerous hydrogen diffusion channels provided by $Na_2Ti_3O_7$ nanotubes, *J. Mater. Chem. A*, 5(2017), No. 13, p. 6178.
[38] Z.L. Ma, J.G. Zhang, Y.F. Zhu, *et al*., Facile synthesis of carbon supported nano-Ni particles with superior catalytic effect on hydrogen storage kinetics of MgH_2, *ACS Appl. Energy Mater.*, 1(2018), No. 3, p. 1158.
[39] Y.Q. Wang, Z.Q. Lan, H. Fu, H.Z. Liu, and J. Guo, Synergistic catalytic effects of ZIF-67 and transition metals (Ni, Cu, Pd, and Nb) on hydrogen storage properties of magnesium, *Int. J. Hydrogen Energy*, 45(2020), No. 24, p. 13376.
[40] Z.Y. Wang, Z.H. Ren, N. Jian, *et al*., Vanadium oxide nanoparticles supported on cubic carbon nanoboxes as highly active catalyst precursors for hydrogen storage in MgH_2, *J. Mater. Chem. A*, 6(2018), No. 33, p. 16177.
[41] H.E. Kissinger, Reaction kinetics in differential thermal analysis, *Anal. Chem.*, 29(1957), No. 11, p. 1702.
[42] P. Wang, Z.H. Tian, Z.X. Wang, *et al*., Improved hydrogen storage properties of MgH_2 using transition metal sulfides as catalyst, *Int. J. Hydrogen Energy*, 46(2021), No. 53, p. 27107.
[43] T. Huang, X. Huang, C. Hu, *et al*., Enhancing hydrogen storage properties of MgH_2 through addition of Ni/$CoMoO_4$ nanorods, *Mater. Today Energy*, 19(2021), art. No. 100613.
[44] N.A. Sazelee, N.H. Idris, M.F. Md Din, *et al*., $LaFeO_3$ synthesised by solid-state method for enhanced sorption properties of MgH_2, *Results Phys.*, 16(2020), art. No. 102844.
[45] Z.W. Ma, S. Panda, Q.Y. Zhang, *et al*., Improving hydrogen sorption performances of MgH_2 through nanoconfinement in a mesoporous CoS nano-boxes scaffold, *Chem. Eng. J.*, 406(2021), art. No. 126790.
[46] S. Hu, H.H. Zhang, Z.L. Yuan, *et al*., Ultrathin $K_2Ti_8O_{17}$ nanobelts for improving the hydrogen storage kinetics of MgH_2, *J. Alloys Compd.*, 881(2021), art. No. 160571.
[47] Y. Wang, L. Li, C.H. An, *et al*., Facile synthesis of TiN decorated graphene and its enhanced catalytic effects on dehydrogenation performance of magnesium hydride, *Nanoscale*, 6(2014), No. 12, art. No. 6684.
[48] M.S. Yahya and M. Ismail, Catalytic effect of $SrTiO_3$ on the hydrogen storage behaviour of MgH_2, *J. Energy Chem.*, 28(2019), p. 46.
[49] M. Avrami, Kinetics of phase change. I general theory, *J. Chem. Phys.*, 7(1939), No. 12, p. 1103.
[50] M.J. Liu, X.Z. Xiao, S.C. Zhao, *et al*., Facile synthesis of Co/Pd supported by few-walled carbon nanotubes as an efficient bidirectional catalyst for improving the low temperature hydrogen storage properties of magnesium hydride, *J. Mater. Chem. A*, 7(2019), No. 10, p. 5277.
[51] W. Zhu, S. Panda, C. Lu, *et al*., Using a self-assembled two-dimensional MXene-based catalyst (2D-Ni@Ti_3C_2) to enhance hydrogen storage properties of MgH_2, *ACS Appl. Mater. Inter.*, 12(2020), No. 45, p. 50333.
[52] L.C. Zhang, K. Wang, Y.F. Liu, *et al*., Highly active multivalent multielement catalysts derived from hierarchical porous $TiNb_2O_7$ nanospheres for the reversible hydrogen storage of MgH_2, *Nano Res.*, 14(2021), No. 1, p. 148.
[53] H.Z. Liu, C.L. Lu, X.C. Wang, *et al*., Combinations of V_2C and Ti_3C_2 MXenes for boosting the hydrogen storage performances of MgH_2, *ACS Appl. Mater. Interfaces*, 13(2021), No. 11, p. 13235.
[54] X. Huang, X.Z. Xiao, W. Zhang, *et al*., Transition metal (Co, Ni) nanoparticles wrapped with carbon and their superior catalytic activities for the reversible hydrogen storage of magnesium hydride, *Phys. Chem. Chem. Phys.*, 19(2017), No. 5, p. 4019.
[55] X. Zhang, Z.H. Leng, M.X. Gao, *et al*., Enhanced hydrogen storage properties of MgH_2 catalyzed with carbon-supported nanocrystalline TiO_2, *J. Power Sources*, 398(2018), p. 183.
[56] M. Zhang, X.Z. Xiao, J.F. Mao, *et al*., Synergistic catalysis in monodispersed transition metal oxide nanoparticles anchored on amorphous carbon for excellent low-temperature dehydrogenation of magnesium hydride, *Mater. Today Energy*, 12(2019), p. 146.
[57] P. Wang, Z.X. Wang, Z.H. Tian, *et al*., Enhanced hydrogen absorption and desorption properties of MgH_2 with NiS_2: The catalytic effect of *in situ* formed MgS and Mg_2NiH_4 phases, *Renewable Energy*, 160(2020), p. 409.
[58] N.S. Norberg, T.S. Arthur, S.J. Fredrick, and A.L. Prieto, Size-dependent hydrogen storage properties of Mg nanocrystals prepared from solution, *J. Am. Chem. Soc.*, 133(2011), No. 28, p. 10679.
[59] W. Liu and K.F. Aguey-Zinsou, Size effects and hydrogen storage properties of Mg nanoparticles synthesised by an electroless reduction method, *J. Mater. Chem. A*, 2(2014), No. 25, art. No. 9718.
[60] T. Liu, H.L. Shen, Y. Liu, *et al*., Scaled-up synthesis of nanostructured Mg-based compounds and their hydrogen storage properties, *J. Power Sources*, 227(2013), p. 86.
[61] T.P. Huang, X. Huang, C.Z. Hu, *et al*., MOF-derived Ni nanoparticles dispersed on monolayer MXene as catalyst for improved hydrogen storage kinetics of MgH_2, *Chem. Eng. J.*, 421(2021), art. No. 127851.